NASA Technical Memorandum 4094

Experimental and Analytical Investigation of the Effect of Spanwise Curvature on Wing Flutter at Mach Number of 0.7

Jose A. Rivera, Jr.

FEBRUARY 1989

NASA

NASA Technical Memorandum 4094

Experimental and Analytical Investigation of the Effect of Spanwise Curvature on Wing Flutter at Mach Number of 0.7

Jose A. Rivera, Jr.
Langley Research Center
Hampton, Virginia

National Aeronautics and
Space Administration
Office of Management
Scientific and Technical
Information Division

1989

Summary

An experimental and analytical study to investigate the effect of spanwise curvature on flutter was conducted at a Mach number of 0.7. Two series of rectangular planform wings of aspect ratio 1.5 and curvature ranging from 0 (uncurved) to 1.04 ft^{-1} were flutter tested in the Langley Transonic Dynamics Tunnel. One series consisted of models with an NACA 65A010 airfoil section; the other, of flat-plate cross-section models. Flutter analyses were conducted for correlation with the experimental results by using structural finite element methods to perform vibration analyses and two aerodynamic theories to obtain unsteady aerodynamic load calculations. The experimental results showed that for one series of models the flutter dynamic pressure increased significantly with curvature, whereas for the other series of models the flutter dynamic pressure decreased with curvature. The flutter analyses, which generally predicted the experimental results, indicated that the difference in behavior of the two series of models was primarily due to differences in their structural properties.

Introduction

Wing and fin designs that are curved (out of plane) spanwise are being used for high-speed missiles at low altitude. These surfaces are curved spanwise so that in the prelaunch position they can fold against the cylindrical missile body (fig. 1). This allows the missile to fit into a launch tube. The possibility of fin flutter is a concern because of the high dynamic pressures at low altitude.

The scientific literature revealed no information relative to the influence of wing spanwise curvature on flutter characteristics. The objective of the present study was to provide analytical and experimental data on generic configurations. Two series of rectangular planform models of aspect ratio 1.5 were flutter tested in the Langley Transonic Dynamics Tunnel (ref. 1). The only difference between models in each series was in curvature (as measured by the reciprocal of the radius of curvature) which ranged from 0 (uncurved) to 1.04 ft^{-1}. The two series of models differed in the airfoil section—the models in one series had NACA 65A010 airfoil sections (fig. 2), whereas the models in the other series had flat-plate airfoil sections with rounded edges. Flutter analyses were conducted for comparison with experimental results using both the planar lifting surface method termed *kernel function* and a nonplanar doublet-lattice method to calculate the unsteady aerodynamic loads.

Symbols

A	peak amplitude of subcritical response data, V
b	wing semispan, measured along the arc length, 2 ft
b_o	wing half-chord, 0.666 ft
C	curvature 1/R, ft^{-1}
EAL	engineering analysis language
f	frequency, Hz
GVT	ground vibration tests
g	structural damping, $\frac{1}{N\pi} \ln \frac{x_o}{x_N}$
M	Mach number
M_o	model mass excluding support, slugs
N	number of cycles
q	dynamic pressure, $\frac{\rho V^2}{2}$, psf
R	radius of curvature, ft
V	velocity, fps
V_I	flutter speed index, $\frac{V}{\omega_\alpha b_o \sqrt{\mu}}$
x_o	reference displacement amplitude, ft
x_N	displacement amplitude after N cycles, ft
ρ	density, $slugs/ft^3$
μ	mass ratio, $\frac{M_o}{\pi b_o^2 b \rho}$
ω_α	first torsion mode frequency, rad/sec

Subscripts:

a	analysis (calculated)
m	measured
F	flutter

Apparatus

Wind Tunnel

The wind-tunnel tests were conducted in the Langley Transonic Dynamics Tunnel (TDT) (ref. 1). The TDT is a continuous-flow, single-return wind tunnel with a 16-ft square test section (with cropped corners) having slots in all four walls. The tunnel is equipped to use either air or Du Pont Freon-12 as the test medium (Freon-12 was used in the present study) at pressures which vary from near vacuum to slightly below atmospheric. The flow is generated by a motor-driven fan. The range of Mach number is

from 0 to 1.2. Both the density and the Mach number are continuously controllable. The TDT is equipped with four hydraulically activated bypass valves that are used to rapidly reduce the Mach number and dynamic pressure in the test section when flutter is encountered.

Models

Geometry. Eight semispan models—four with NACA 65A010 airfoil sections and four with flat-plate cross sections—were tested. Values of curvature (the reciprocal of the radius of curvature) were 0 (uncurved), 0.625, 0.787, and 1.04 ft^{-1}. The models had a semispan or arc length of 2.0 ft and a chord of 1.33 ft resulting in an aspect ratio of 1.5. The planform geometry and the radii are shown in figure 3.

Construction. The flat-plate models were constructed of 0.09-in-thick 6061-T6 aluminum-alloy sheet. The leading and trailing edges were rounded, and the aluminum sheet was bent to the appropriate curvatures. The NACA 65A010 airfoil section models were constructed of 0.09-in-thick 6061-T6 aluminum-alloy plate to which a lightweight (1.5 lb/ft^3) foam was attached and shaped to give the desired airfoil shape. The foam was attached to the curved aluminum in precut strips with double-back adhesive tape, and the surface roughness was smoothed with a mixture of latex paint and filler material. High-strength tape was added along the leading and trailing edges of the models and also on the wingtip to avoid foam separation due to airloads at these critical locations. A 0.2-in-wide strip of No. 30 Carborundum grit was added along the 5-percent chord line of the upper and lower wing surfaces to provide the desired flow transition characteristics. The grit size and location were based on previous experience with other wind-tunnel models.

Each model was instrumented with two strain-gauge bridges that were attached to the aluminum plate near the wing root. The two bridges were oriented to be sensitive to bending and torsional strains, respectively.

Model Mount

A photograph showing the uncurved 65A010 model mounted in the wind tunnel is presented in figure 4. The models were cantilever mounted outside the tunnel-wall boundary layer on a 4-in-deep I-beam support fixture attached to a remotely controlled turntable. The turntable provided the capability of changing the wing model angle of attack during the test (fig. 5). A 4- by 3-ft splitter plate was mounted to the support fixture to provide a reflection plane. Wool tufts 3 in. long were attached to the splitter plate for flow visualization. During wind-on tests, the tuft patterns indicated there was relatively undisturbed flow over the splitter plate.

Model Structural Modes

Measured Structural Modes

The first four natural frequencies (first bending, first torsion, second bending, and second torsion) were measured for each model. The models were excited by using a pulsed jet air shaker, and frequencies were obtained by analyzing the output signals from the strain-gauge bridges with a frequency analyzer. Measured frequencies for each model are presented in table 1. For the measured frequencies, the frequency ratio (f_2/f_1) decreased with curvature for each set of models. During the ground vibration tests (GVT), a change in character of the first torsion mode shape was noticed. Due to the inboard torsional motion of the wing associated with the first torsion mode, the outboard motion became primarily chordwise as model curvature increased (fig. 6). This phenomenon was noticed during the GVT measurements and was observed to be typical behavior for the curved models. Structural damping values for the first bending and first torsion modes were obtained from the GVT. For the NACA 65A010 models these values are presented in table 1 and were used in calculating the flutter results.

Analytical Structural Modes

A dynamic analysis using the engineering analysis language (EAL), finite element, structural analysis program (ref. 2) provided mode shapes, generalized mass, and natural frequencies for the first four modes of vibration. The mode shapes and generalized masses were used in the flutter analyses, and the calculated natural frequencies f_a were used for correlation with the GVT-measured frequencies f_m (table 1). The calculated node lines for the first three modes of the NACA 65A010 models are shown in figure 7 (node lines for the flat-cross-section models were similar) and were substantiated by measurements during the GVT. Figure 8 presents the measured and calculated node lines for NACA 65A010 model 2 ($C = 0.625$ ft^{-1}). In summary, the calculated results correlated well with the GVT results. The finite element models consisted of 108 two-dimensional quadrilateral plate elements having both membrane and bending stiffness (fig. 9). The 108 element configuration consisted of 9 elements chordwise and 12 spanwise. Only the normal components of modal deflections were used in the

flutter analysis. These were the radial components for the curved models. (See fig. 10.) These deflections were also used to assess the mode shapes.

Flutter Analysis

Unsteady Aerodynamic Forces

Flutter analyses were performed by using two unsteady aerodynamic methods. These methods considered the wings to be thin flat plates (no airfoil cross section). For the present purposes one is termed the *kernel-function method*, and the other is termed the *doublet-lattice method* even though it has its own kernel function that relates a lifting line of doublets to the downwash. The kernel-function method originated from Watkins, Woolston, and Cunningham (ref. 3), and its computer program is described by Desmarais and Bennett (ref. 4). Notably this program uses the planar kernel for an uncurved wing; thus, each span station is analyzed as if it were part of an uncurved wing. In contrast the doublet-lattice method of Giesing, Kalman, and Rodden (ref. 5) includes the nonplanar kernel so that the out-of-plane curvature of the present models can be directly modeled.

Kernel-function method. The FAST computer program described in reference 4 was used to obtain the kernel-function unsteady aerodynamic forces. This program uses a surface spline (ref. 6) to interpolate the displacements and slopes at the downwash collocation points from the calculated mode shapes. Figure 11 shows the 36 collocation points—6 points chordwise at each of 6 span stations used for these analyses.

Doublet-lattice method. The doublet-lattice method is directly applicable to curved panels. From the ISAC assembly of programs (ref. 7), the aerostructural interface program DLIN and the doublet-lattice method (ref. 5) of program DLAT were used. Program DLIN utilizes the surface-spline interpolation technique (ref. 6) to obtain deflections and slopes on aerodynamic boxes from deflections at structural nodes. Program DLAT computes the generalized aerodynamic forces. Figure 11 shows the 96 uniform aerodynamic boxes—8 boxes chordwise at each of 12 spanwise locations.

Flutter Computation Routines

Program FLUTDET of the FAST routine (ref. 4) was used to solve the flutter eigenvalue problem. Unsteady aerodynamics calculated by both aerodynamic theories (planar kernel function and doublet lattice) were used by program FLUTDET (in separate analyses) to calculate flutter speeds at $M = 0.7$ and various densities using the traditional incremental damping approach (V-G method). From these calculations, matched point solutions for flutter dynamic pressure and flutter speed index were obtained. (Flutter speed index, defined as $V/(\omega_\alpha b_o \sqrt{\mu})$, is a nondimensional quantity typically used to compare parametric changes. The flutter speed index largely disassociates mass, stiffness, and scale effects from the planform or configuration being studied.)

Wind-Tunnel Tests

Data Analysis

The wind-tunnel data acquisition system (ref. 8) was used to calculate, record, and display tunnel parameters and model loads. The output signals from the model strain-gauge bridges were monitored on strip chart recorders. Model frequencies and peak response amplitudes were determined by using a frequency analyzer. The peak hold subcritical response method (ref. 9) was used to predict flutter onset during the test. This method uses data acquired by the frequency analyzer, which displays a continuously updated frequency spectrum of the response amplitude. Flutter onset is predicted by tracking the inverse of the response amplitude 1/A versus dynamic pressure q for a given mode. Then 1/A is extrapolated to 0 to predict the flutter q before it is reached.

Test Procedure

With the wind tunnel evacuated to a low density, the tunnel velocity was slowly increased until a Mach number of 0.7 was reached. Subcritical response data were collected at this tunnel condition. Next, while holding the Mach number at 0.7, the test-section dynamic pressure was increased in incremental steps by adding Freon-12 into the wind tunnel. At selected dynamic pressures, tunnel flow conditions were held constant, and subcritical response data were recorded. This process was repeated until flutter was actually encountered or until sufficient subcritical data were obtained to predict the flutter dynamic pressure by an extrapolation technique. The models were tested with the angle of attack adjusted to keep the lift force equal to the weight of the model. This corresponded to an angle-of-attack range of about 2° for the NACA 65A010 models and about 1/2° for the flat-plate models.

Results and Discussion

Two flutter analysis methods were used for the models in this investigation—a kernel-function method and a doublet-lattice method. These

methods are identified by the aerodynamic theories used to calculate the unsteady aerodynamic forces. Each method used the calculated displacements perpendicular to the model in the unsteady aerodynamic load calculations. The analyses for the NACA 65A010 models utilized measured natural frequencies and structural damping from the GVT. A plot showing the effect of structural damping on the NACA 65A010 results is shown in figure 12. The large values of damping had a significant effect on the results and thus were included in the analysis. The flutter analyses of the flat-plate cross-section wing model were conducted by using measured natural frequencies from the GVT and a value of 0 for structural damping. Damping was observed to be much less than that for the NACA 65A010 models and was not measured for these models.

The four NACA 65A010 models and the four models with the flat cross section were flutter tested in Freon-12 at $M = 0.7$.

NACA 65A010 Models

Analytical results. The kernel-function results are presented in table 2(a) and figure 13. The flutter speed index shows an increase as curvature increases. These results also show that flutter dynamic pressure increases with curvature. Flutter frequency ratios, which are also shown in the figure, indicate there was not a significant change in modal participation as curvature increases. The kernel-function method incorporates the mode shape and frequency effects on flutter due to curvature but the kernel-function aerodynamic theory is a planar lifting surface routine. Therefore, the aerodynamic effects on flutter due to the wing curvature are not included in this method. The results of these analyses show the curvature effects on flutter due to the change in unsteady aerodynamic loads. The change in unsteady aerodynamic loads is associated with the changing structural dynamic behavior (mode shapes and frequency) which accompany varying curvature. This change in structural dynamic behavior was mentioned previously and is characterized by a change from torsional motion to in-plane or fore-and-aft motion of the outboard section of the wing model. The flutter speed index and dynamic pressure increase as this change occurs because less energy is obtained from the airstream as the torsional motion decreases in perpendicular amplitude.

The doublet-lattice results are presented in tables 2(b) and figure 13 and show an increase in flutter speed index and flutter dynamic pressure as curvature increases. Changes in the structural dynamic behavior which accompany curvature are believed to cause the overall increase in flutter speed. Flutter frequency ratios are also presented and show no significant change in modal participation. These analyses, like the kernel-function analyses, indicate increases in flutter speed index and flutter dynamic pressure, but the increase in flutter dynamic pressure is less. Because the analyses are nonplanar and account for the aerodynamics on the curved surface, this smaller increase in flutter dynamic pressure may be attributed to an aerodynamic effect caused by the model curvature. It appears that curvature causes the aerodynamics to decrease flutter dynamic pressure or oppose the effect of the change in character of the torsional mode shape.

Experimental results. The basic experimental flutter results are presented in table 3. The flutter dynamic pressure, flutter speed index, and flutter frequency ratio for each NACA 65A010 model are presented in figure 14. The flutter frequency ratio increased slightly with curvature. The flutter dynamic pressure and flutter speed index also increased as curvature increased. The change in character of the first torsion mode shape to in plane at the tip (fig. 6) is believed to cause this effect.

Comparison of experiment and analysis. Basic experimental and analytical flutter results for the NACA 65A010 model are given in tables 2 and 3. The NACA 65A010 wind-tunnel test results, the kernel-function analyses, and the doublet-lattice analysis all show an increase in flutter dynamic pressure as curvature increases (fig. 15). When compared with the NACA 65A010 experimental results, the kernel-function analysis flutter prediction is conservative and becomes nonconservative as the curvature increases. The trend to become unconservative with curvature is attributed to the planar nature of the analysis. The doublet-lattice analysis flutter predictions remain conservative throughout the range of investigated curvatures because the flutter dynamic pressure decreasing effects of curvature are included.

Flat-Plate Cross-Section Models

Analytical results. The kernel-function results are presented in table 4(a) and figure 16. These analyses predicted an increase in flutter speed index and a small increase in flutter dynamic pressure. Because the analysis is planar, the calculated increases are due to the changes in structural dynamic behavior with curvature.

The doublet-lattice basic analytical results are presented in table 4(b) and figure 16. These results

show an increase in flutter speed index and a relatively constant flutter dynamic pressure with increasing curvature. Here the aerodynamic effect due to curvature appears to have offset the structural dynamic effect that is evident in the kernel-function results.

Experimental results. The basic experimental flutter results are presented in table 3(b) and figure 17. The figure shows the variations with curvature of the flutter dynamic pressure, the flutter speed index, and the flutter frequency ratio. The flutter speed index increased with curvature as with the 65A010 models. The flutter frequency ratio also increased slightly with curvature. The flutter dynamic pressure decreased with curvature between the model with no curvature ($C = 0$) and the model with the least amount of curvature ($C = 0.625$). From this point on ($0.625 < C < 1.04$), the flutter dynamic pressure is nearly constant with curvature. The flat-plate cross-section models did exhibit the change in character of the first torsion mode shape to in plane at the tip with curvature during the GVT yet the flutter dynamic pressure did not increase. Analysis indicates that curvature causes the aerodynamics to decrease flutter dynamic pressure. This effect may have countered the effect of the change in character of the first torsion mode strongly enough to cause an overall decrease in flutter dynamic pressure.

Comparison of experiment and analysis. The flat-plate cross-section experimental results show a decrease in flutter dynamic pressure with curvature (fig. 18) between the model with no curvature ($C = 0$) and the model with the least amount of curvature ($C = 0.625$). At higher curvature, the flutter dynamic pressure remains practically constant. The kernel-function analysis predicts a consistent increase in flutter dynamic pressure with curvature that is conservative at zero curvature and becomes unconservative with curvature. The doublet-lattice analysis compares more favorably with the experiment results than the kernel-function analysis. This is attributed to the effects of geometry that are considered in the analysis. The analysis shows a very small increase in flutter dynamic pressure with curvature between the model with no curvature ($C = 0$) and the model with the least curvature ($C = 0.625$). This trend opposes the measured trend. For higher curvature, the analysis predicts a slightly decreasing flutter dynamic pressure with curvature that compares well with the experimental results although somewhat unconservative. The doublet-lattice analysis is conservative at zero curvature and becomes unconservative with curvature.

Comparison of the Two Series of Models

The experimental results for the models with NACA 65A010 airfoil sections showed an increase in flutter dynamic pressure as curvature increased. The models with the flat-plate airfoil sections showed a decrease in flutter dynamic pressure as curvature increased. The flutter analyses using either kernel-function (planar) or doublet-lattice (nonplanar) aerodynamics generally predicted the flutter dynamic pressure for both series of models. The doublet-lattice results, which included the aerodynamic effects of curvature, showed better agreement with experimental results. Since the analyses considered the wings to be thin plates, they clearly indicated that the difference in trend for the two series of models was due primarily to differences in structural properties. In other words, airfoil shape was not shown to be a significant factor.

Conclusions

An experimental and analytical study has been conducted in the Langley Transonic Dynamic Tunnel to investigate the effects of spanwise curvature on the flutter characteristics of a generic wing. Two series of rectangular planform wing models of panel aspect ratio 1.5 were investigated. The first series of wings had an NACA 65A010 airfoil section, the second series of wings had a flat-plate cross section. For each series the same four values of spanwise curvature were investigated. The curvature ranged from 0 (uncurved) to 1.04 ft^{-1}. The results are summarized as follows:

1. The wind-tunnel experimental results for the models with NACA 65A010 airfoil sections showed an increase in flutter dynamic pressure as curvature increased. This was primarily due to the change in character of the first torsion mode.

2. The flutter analyses for the NACA 65A010 models using either kernel-function (planar) or doublet-lattice (nonplanar) aerodynamics generally predicted the effects of curvature. Both analyses were slightly conservative at zero curvature. The kernel-function analyses were slightly unconservative with curvature. The doublet-lattice analyses remained slightly conservative with curvature.

3. Comparison of the kernel-function (planar) and doublet-lattice (nonplanar) analyses indicated a structural dynamic and an aerodynamic effect on flutter caused by curvature of the models in this study. The structural dynamic effect which changed the character of the first torsion mode shape increased flutter dynamic pressure, whereas the aerodynamic effect caused by curvature of the wing appeared to reduce the flutter dynamic pressure.

4. The wind-tunnel experimental results for the models with flat-plate airfoil sections showed a decrease in flutter dynamic pressure with curvature. These models did exhibit the structural dynamic change in character of the first torsion mode to in plane. The aerodynamics caused by curvature may have countered the effect of this structural dynamic change to cause an overall decrease in flutter dynamic pressure.

5. The flutter analyses for the flat-plate models using either kernel-function (planar) or doublet-lattice (nonplanar) aerodynamics predicted results that were slightly conservative for the uncurved model. Neither analysis predicted the overall decrease in flutter dynamic pressure with curvature that was measured for the models, and both predictions were unconservative with curvature.

6. The flutter analyses indicated that the difference in trend for the two series of models was due primarily to differences in structural properties. In other words, airfoil shape was not shown to be a significant factor.

NASA Langley Research Center
Hampton, VA 23665-5225
December 20, 1988

References

1. Reed, Wilmer H., III: *Aeroelasticity Matters: Some Reflections on Two Decades of Testing in the NASA Langley Transonic Dynamics Tunnel.* NASA TM-83210, 1981.
2. Whetstone, W. D.: *EISI-EAL Engineering Analysis Language Reference Manual—EISI-EAL System Level 2091. Volume 1: General Rules and Utility Processors.* Engineering Information Systems, Inc., July 1983.
3. Watkins, Charles E.; Woolston, Donald S.; and Cunningham, Herbert J.: *A Systematic Kernel Function Procedure for Determining Aerodynamic Forces on Oscillating or Steady Finite Wings at Subsonic Speeds.* NASA TR R-48, 1959.
4. Desmarais, Robert N., and Bennett, Robert M.: *User's Guide for a Modular Flutter Analysis Software System (FAST Version 1.0).* NASA TM-78720, 1978.
5. Giesing, J. P.; Kalman, T. P.; and Rodden, W. P.: *Subsonic Unsteady Aerodynamics for General Configurations.* U.S. Air Force, Nov. 1971.
   Part I, Volume I—Direct Application of the Nonplanar Doublet-Lattice Method. AFFDL-TR-71-5, Pt. I, Vol. I. (Available from DTIC as AD 891 403L.)
   Part I, Volume II—Computer Program H7WC. AFFDL-TR-71-5, Pt. I, Vol. II. (Available from DTIC as AD 892 535L.)
6. Harder, Robert L.; and Desmarais, Robert N.: Interpolation Using Surface Splines. J. Aircr., vol. 9, no. 2, Feb. 1972, pp. 189–191.
7. Peele, Ellwood L.; and Adams, William M., Jr.: *A Digital Program for Calculating the Interaction Between Flexible Structures, Unsteady Aerodynamics and Active Controls.* NASA TM-80040, 1979.
8. Cole, Patricia H.: *Wind Tunnel Real-Time Data Acquisition System.* NASA TM-80081, 1979.
9. Sandford, Maynard C.; Abel, Irving; and Gray, David L.: *Development and Demonstration of a Flutter-Suppression System Using Active Controls.* NASA TR R-450, 1975.

Table 1. Wing Model Analytical and Measured Properties

Model	R, ft	C, ft^{-1}	M_o, slugs	f_2/f_1	Mode 1 1st bending f_a, Hz	Mode 1 1st bending f_m, Hz	Mode 1 1st bending g_m	Mode 2 1st torsion f_a, Hz	Mode 2 1st torsion f_m, Hz	Mode 2 1st torsion g_m	Mode 3 2nd bending f_a, Hz	Mode 3 2nd bending f_m, Hz	Mode 3 2nd bending g_m	Mode 4 2nd torsion f_a, Hz	Mode 4 2nd torsion f_m, Hz	Mode 4 2nd torsion g_m
(a) NACA 65A010 models																
1	∞	0.0	0.1264	3.96	4.9	4.8	0.056	18.2	19.0	0.07	30.5	31.2		60.0	65.8	
2	1.6	.625	.128	3.28	5.0	5.0	.03	15.3	16.4	.055	26.0	27.2		42.1	47.2	
3	1.27	.787	.128	3.04	5.1	4.9	.038	14.5	14.9	.056	24.7	25.6		39.6	42.8	
4	.96	1.04	.129	2.72	5.3	5.1	.04	13.0	13.9	.071	22.1	22.7		36.2	40.4	
(b) Flat-plate cross-section models																
1	∞	0.0	0.111	3.58	5.35	4.8		17.85	17.2		33.2	31.2		60.42	60.0	
2	1.6	.625	.112	2.83	5.56	5.4		15.27	15.3		29.08	28.4		42.49	42.4	
3	1.27	.787	.111	2.61	5.76	5.4		14.56	14.1		27.78	26.0		39.96	39.6	
4	.96	1.04	.111	2.25	5.97	5.6		13.28	12.6		24.97	23.2		36.52	34.8	

Table 2. Calculated Flutter Results for NACA 65A010 Cross Section at $M = 0.7$

Model	C, ft^{-1}	M	V, fps	ρ, slugs/ft^3	q, psf	μ	$\sqrt{\mu}$	V_I	f_F, Hz	f_F/f_2	f_2, Hz	ω_α, rad/sec	M_o, slugs	Aero	Modes	f, Hz	g
(a) Kernel-function analyses																	
1	0.0	0.7	350	0.00137	83.9	33.2	5.76	0.765	8.38	0.441	19.0	119.4	0.1264	Kernel	4	f_m	g_m
2	.625	.7	350	.00166	101.7	27.8	5.27	.969	8.8	.537	16.4	103.0	.128	Kernel	4	f_m	g_m
3	.787	.7	350	.0017	104.1	27.1	5.21	1.08	8.47	.568	14.9	93.6	.128	Kernel	4	f_m	g_m
4	1.04	.7	350	.00228	139.7	20.3	4.51	1.34	8.58	.617	13.9	87.3	.129	Kernel	4	f_m	g_m
(b) Doublet-lattice analyses																	
1	0.0	0.7	350	0.00129	79.0	35.2	5.93	0.742	8.62	0.454	19.0	119.4	0.1264	DLAT	4	f_m	g_m
2	.625	.7	350	.00147	90.0	31.2	5.59	.914	9.14	.557	16.4	103.0	.128	DLAT	4	f_m	g_m
3	.787	7	350	.00149	91.3	30.9	5.56	1.008	8.84	.593	14.9	93.8	.128	DLAT	4	f_m	g_m
4	1.04	.7	350	.00185	113.3	25.1	5.01	1.203	8.96	.645	13.9	87.3	.129	DLAT	4	f_m	g_m

Table 3. Experimental Flutter Results

Model	C, ft^{-1}	M	V, fps	ρ, slugs/ft^3	q, psf	μ	$\sqrt{\mu}$	V_I	f_F, Hz	F_F/f_2	f_2, Hz	ω_2, rad/sec	M_o, slugs
(a) NACA 65A010 models													
1	0.0	0.701	348.8	0.00153	93.1	29.6	5.44	0.806	10.0	0.526	19.0	119.4	0.1264
2	.625	.707	353.4	.001495	93.4	30.7	5.54	.930	10.3	.628	16.4	103.0	.128
3	.787	.700	349.9	.001683	103.0	27.3	5.22	1.075	9.6	.644	14.9	93.6	.128
4	1.04	.706	352.2	.002064	128.0	22.4	4.74	1.278	10.3	.741	13.9	87.3	.129
(b) Flat-plate cross-section models													
1	0.0	0.706	353.9	0.001012	63.4	39.4	6.27	0.784	10.4	0.605	17.2	108.1	0.111
2	.625	.705	350.7	.000791	48.6	50.8	7.13	.769	10.0	.654	15.3	96.1	.112
3	.787	.701	348.7	.000812	49.4	49.0	7.00	.844	9.8	.695	14.1	88.6	.111
4	1.04	.703	349.8	.000813	49.7	49.0	7.00	.947	9.5	.754	12.6	79.2	.111

Table 4. Calculated Flutter Results for Flat-Plate Cross Section at $M = 0.70$

Model	C, ft^{-1}	M	V, fps	ρ, slugs/ft^3	q, psf	μ	$\sqrt{\mu}$	V_I	f_F, Hz	f_F/f_2	f_2, Hz	ω_α, rad/sec	M_o, slugs	Aero	Modes	f, Hz	g
(a) Kernel-function analyses																	
1	0.0	0.7	350	0.000859	52.6	46.4	6.81	0.714	9.18	0.534	17.2	108.07	0.111	Kernel	4	f_m	0
2	.625	.7	350	.001058	64.8	38.0	6.16	.887	9.48	.620	15.3	96.13	.112	Kernel	4	f_m	0
3	.787	.7	350	.001051	64.4	37.9	6.16	.963	9.25	.656	14.1	88.59	.111	Kernel	4	f_m	0
4	1.04	.7	350	.001136	69.6	35.1	5.92	1.121	9.12	.724	12.6	79.17	.111	Kernel	4	f_m	0
(b) Doublet-lattice analyses																	
1	0.0	0.7	350	0.000800	49.0	49.8	7.06	0.689	9.50	0.552	17.2	108.07	0.111	DLAT	4	f_m	0
2	.625	.7	350	.000914	56.0	44.0	6.63	.825	9.87	.645	15.3	96.13	.112	DLAT	4	f_m	0
3	.787	.7	350	.000887	54.3	44.9	6.70	.885	9.66	.685	14.1	88.59	.111	DLAT	4	f_m	0
4	1.04	.7	350	.000873	53.5	45.6	6.75	.983	9.52	.756	12.6	79.17	.111	DLAT	4	f_m	0

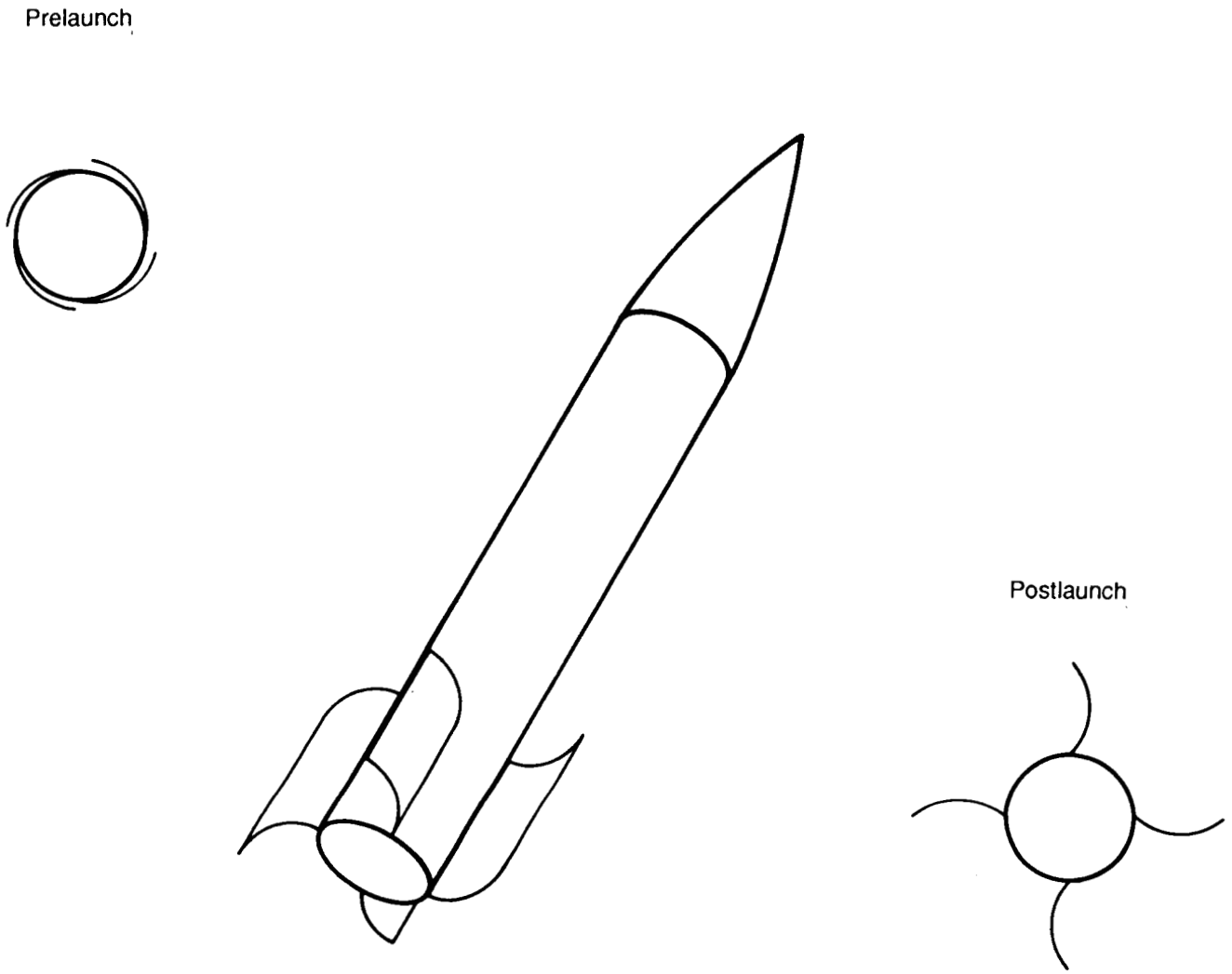

Figure 1. Spanwise curvature fins on missile afterbody.

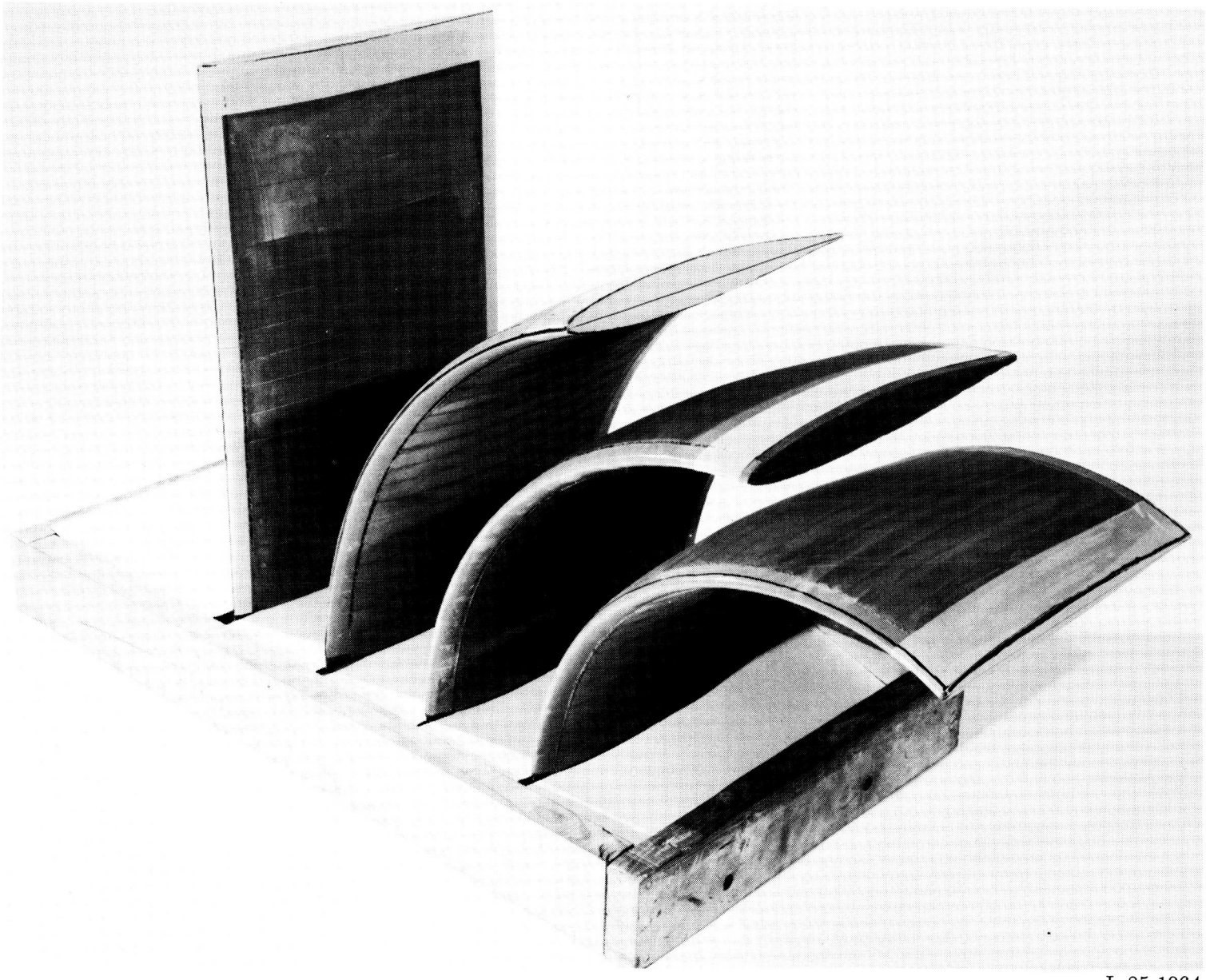

L-85-1064

Figure 2. NACA 65A010 spanwise curvature models.

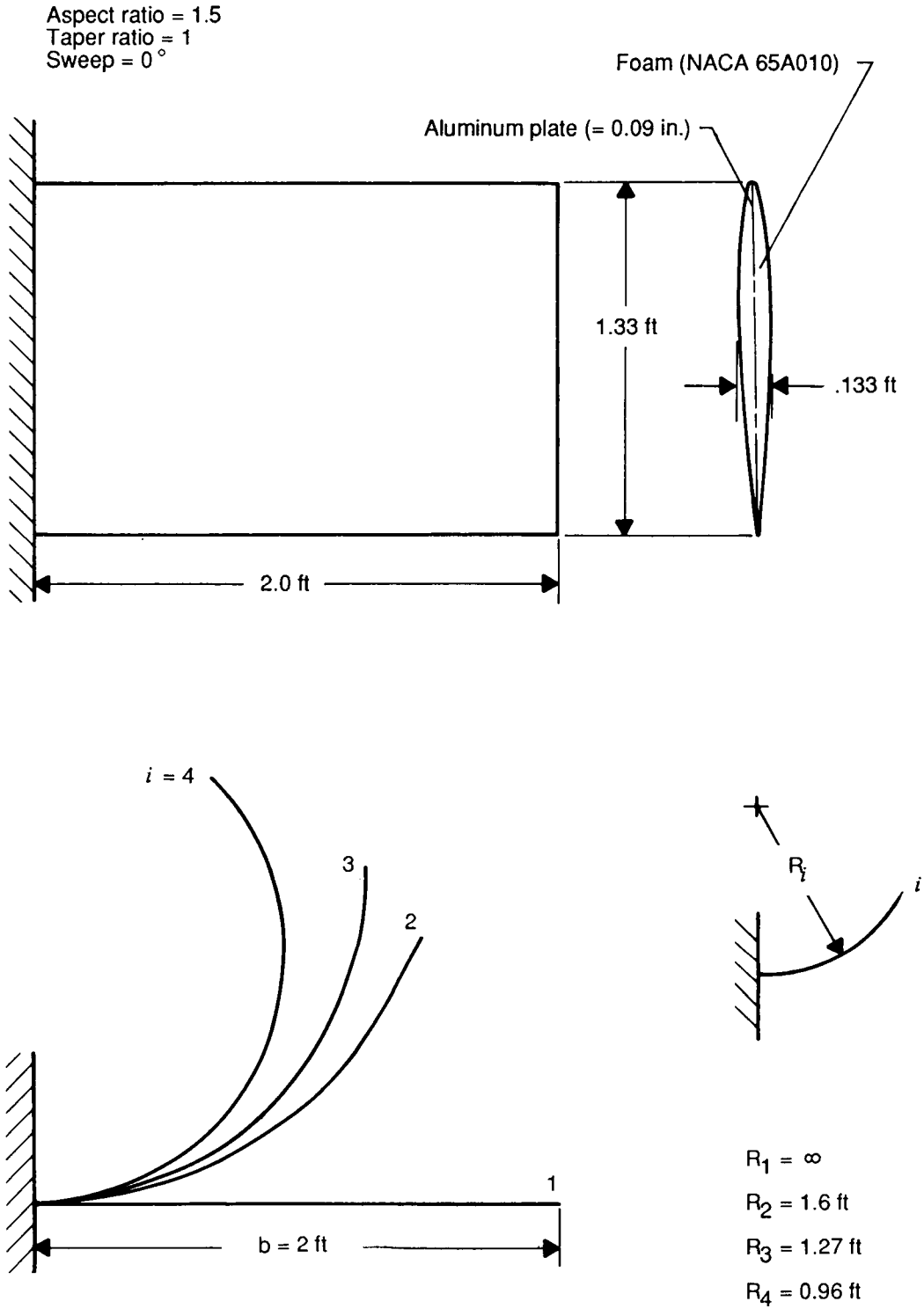

Figure 3. Model geometry.

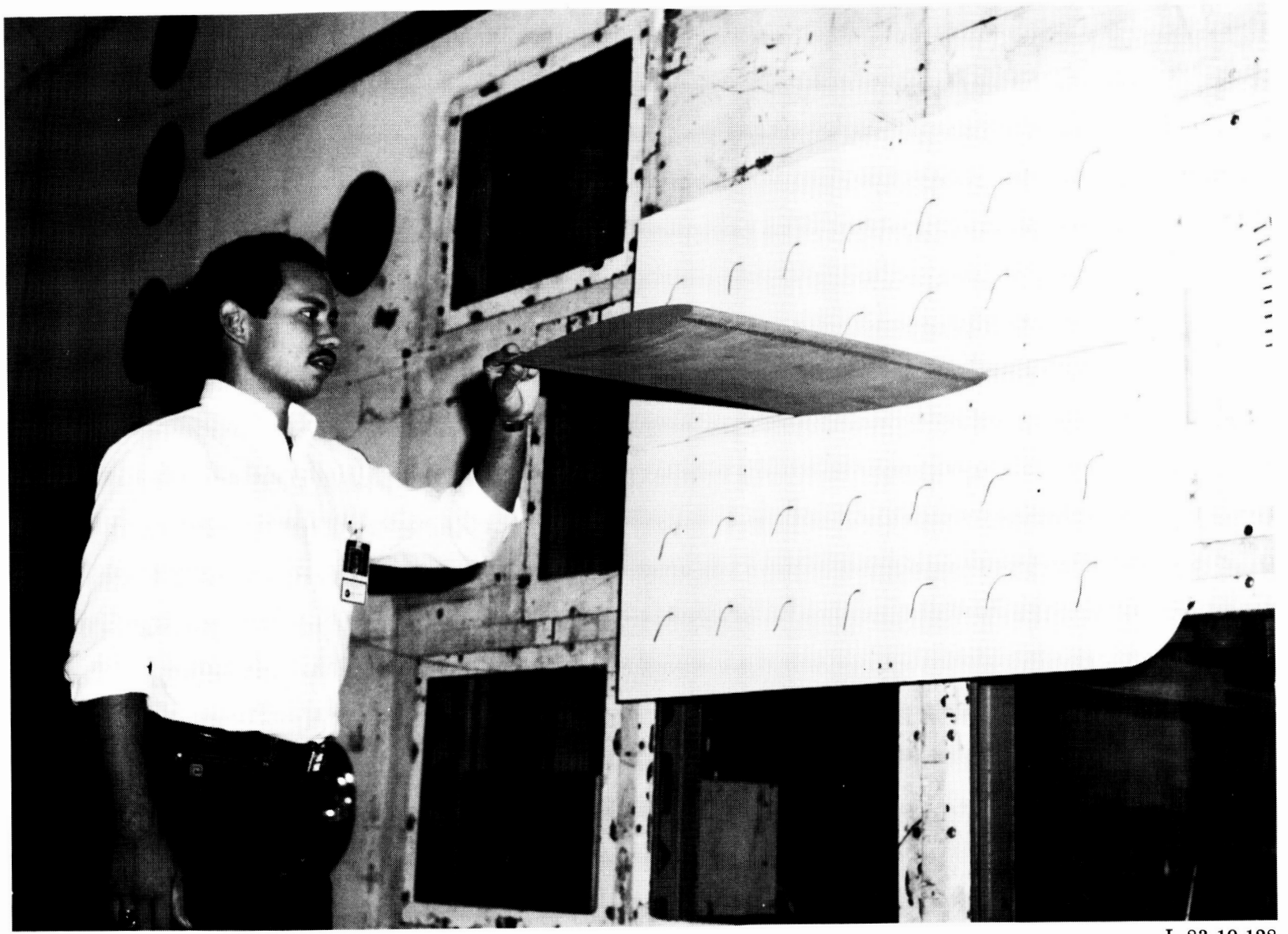

L-83-10,128

Figure 4. Uncurved NACA 65A010 spanwise curvature model mounted in TDT.

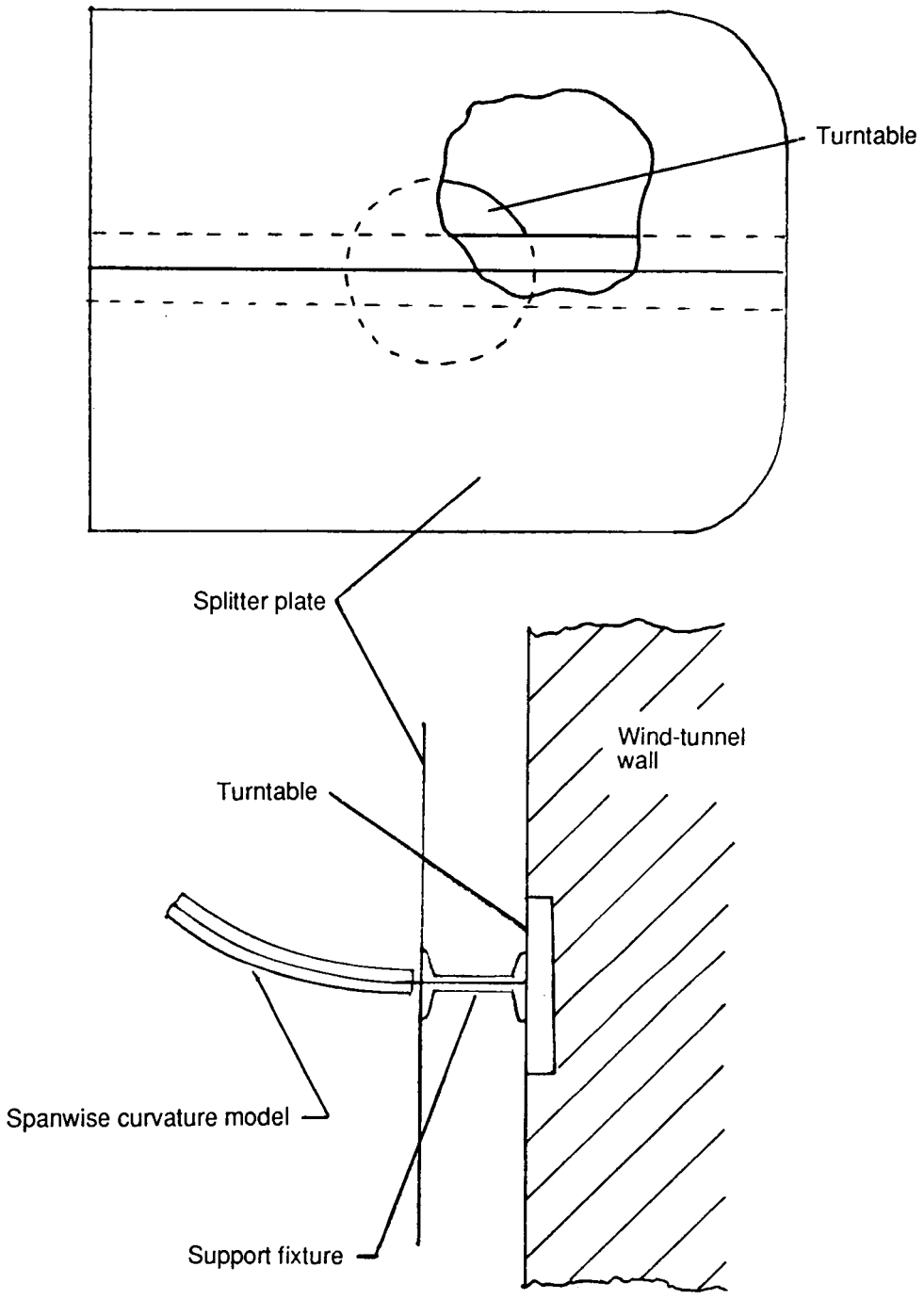

Figure 5. Sketch of model support fixture with splitter plate.

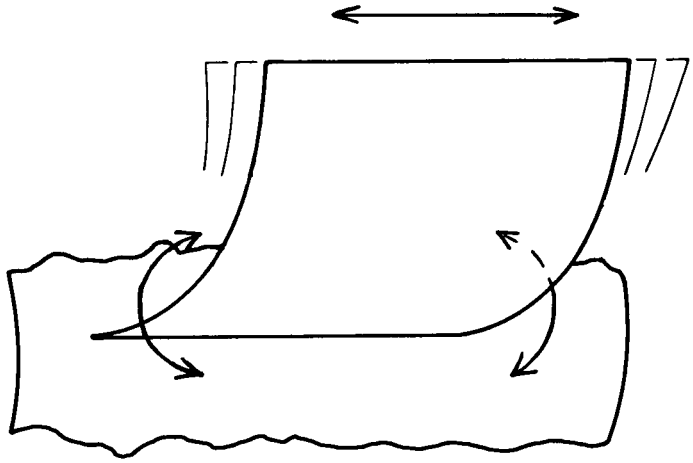

Figure 6. Inboard torsional motion in first torsional mode (curved arrows) and associated outboard in-plane motion.

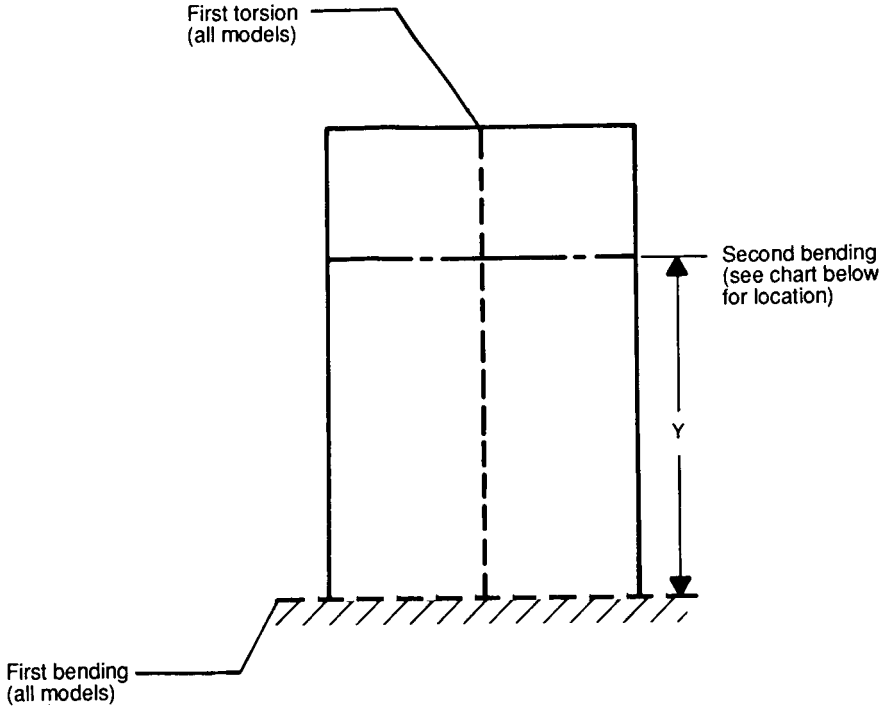

Second bending node line location chart

Mode	Curvature, ft-1	Y, ft
1	0.0	1.06
2	0.625	1.00
3	0.787	0.97
4	1.04	0.93

Figure 7. Calculated node lines for first three modes of NACA 65A010 spanwise curvature models (Y measured along surface).

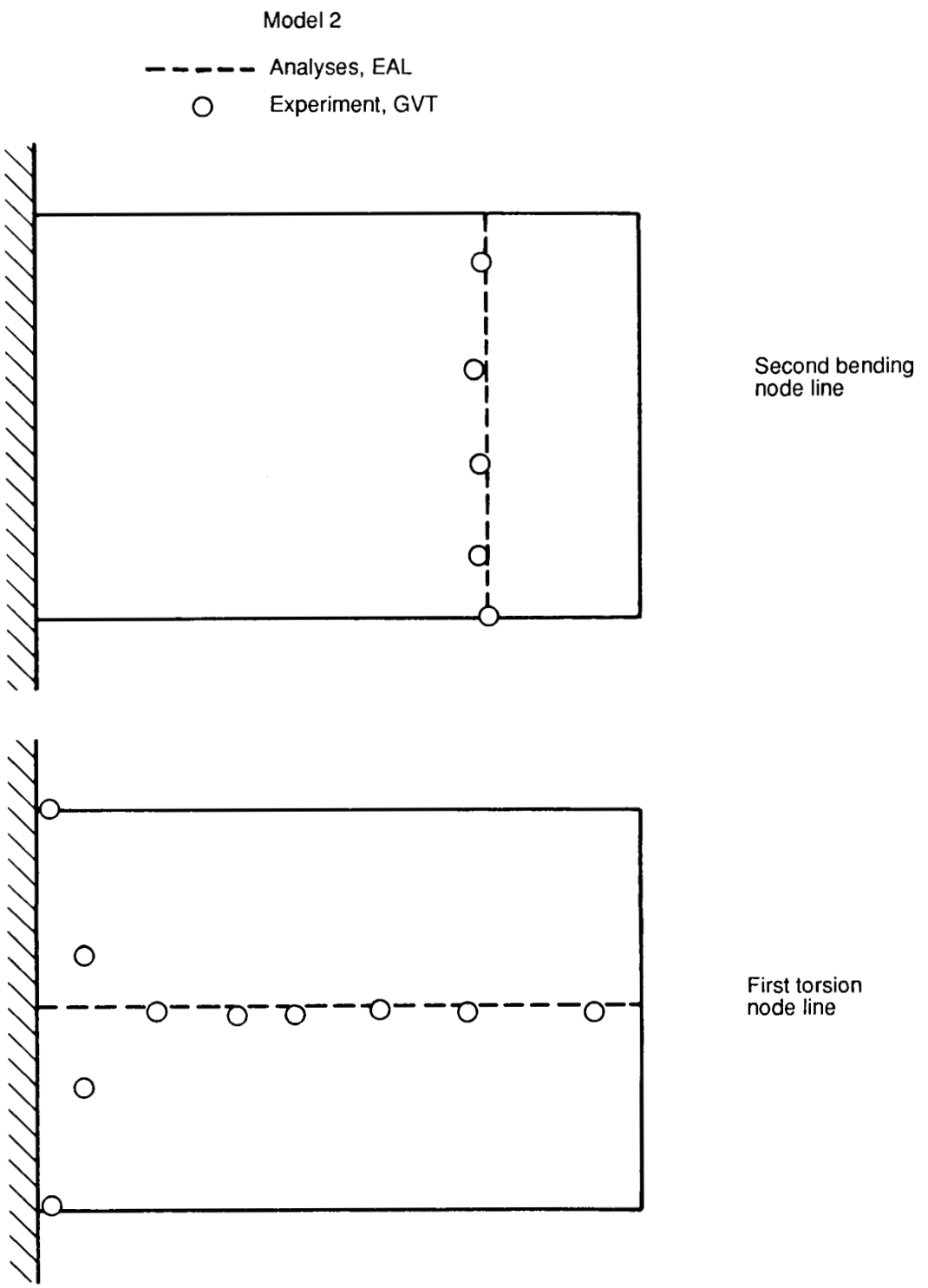

Figure 8. Experimental and calculated node lines for NACA 65A010 model. $C = 0.625$ ft^{-1}.

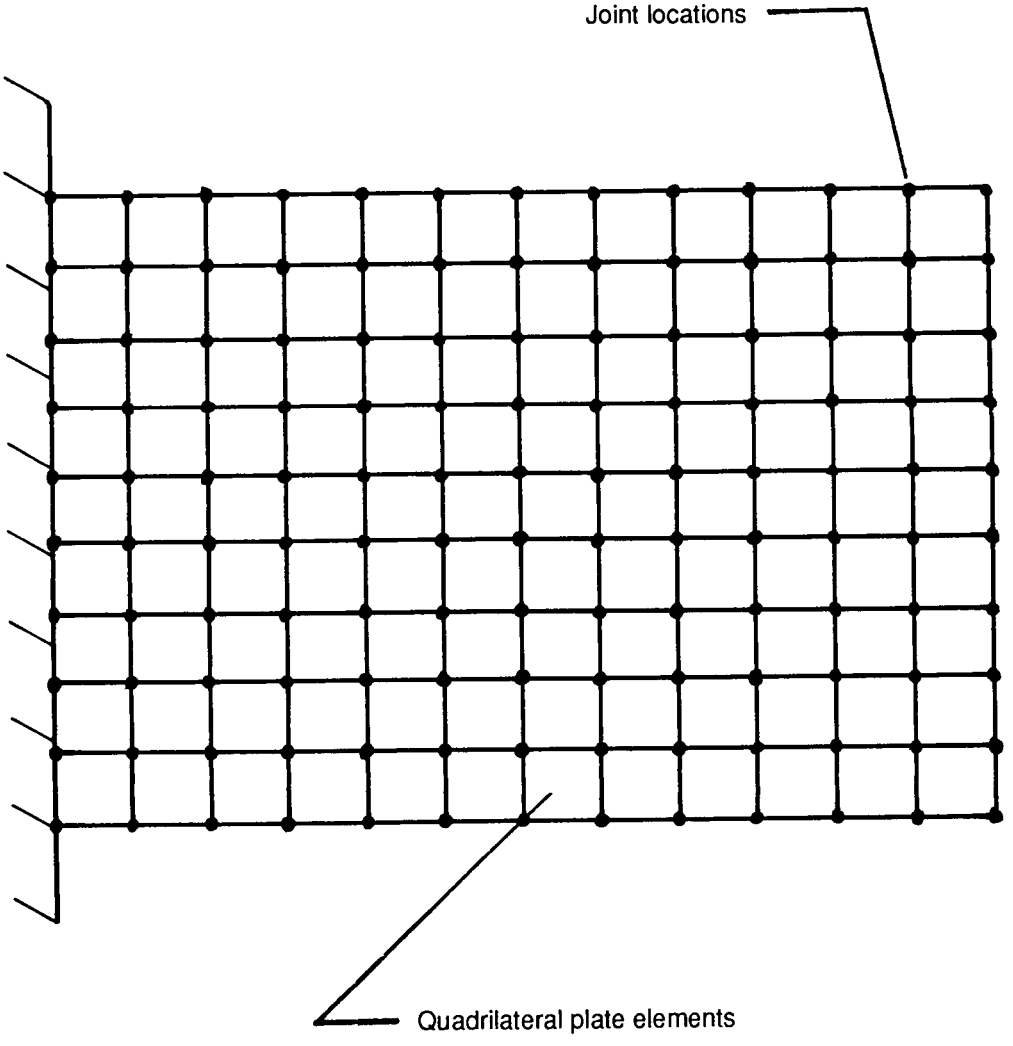

Figure 9. EAL structural model.

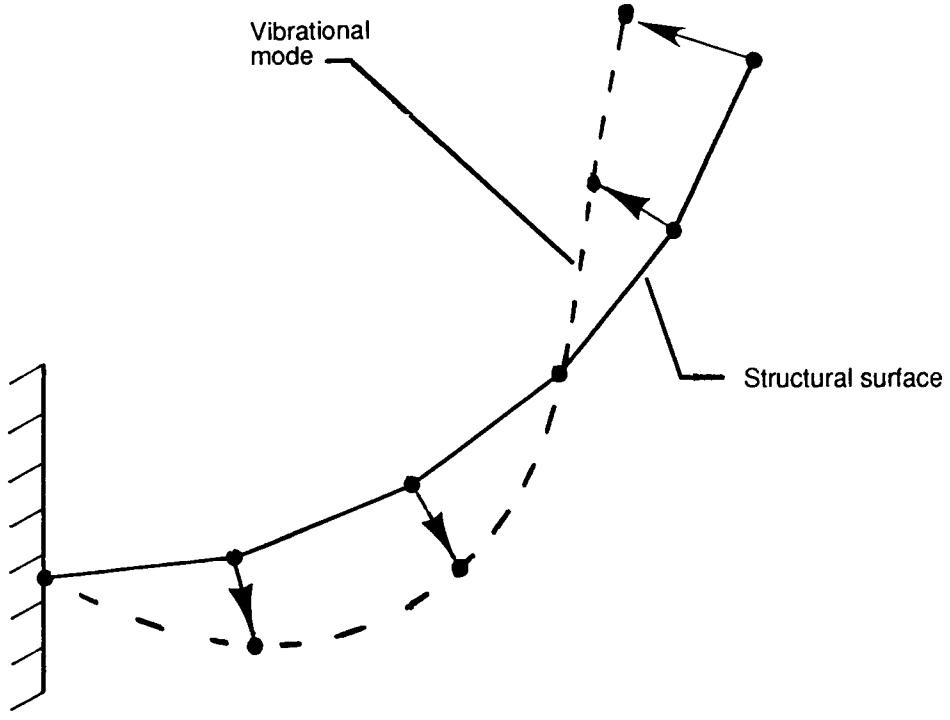

Figure 10. Sketch showing modal joint deflections perpendicular to surface.

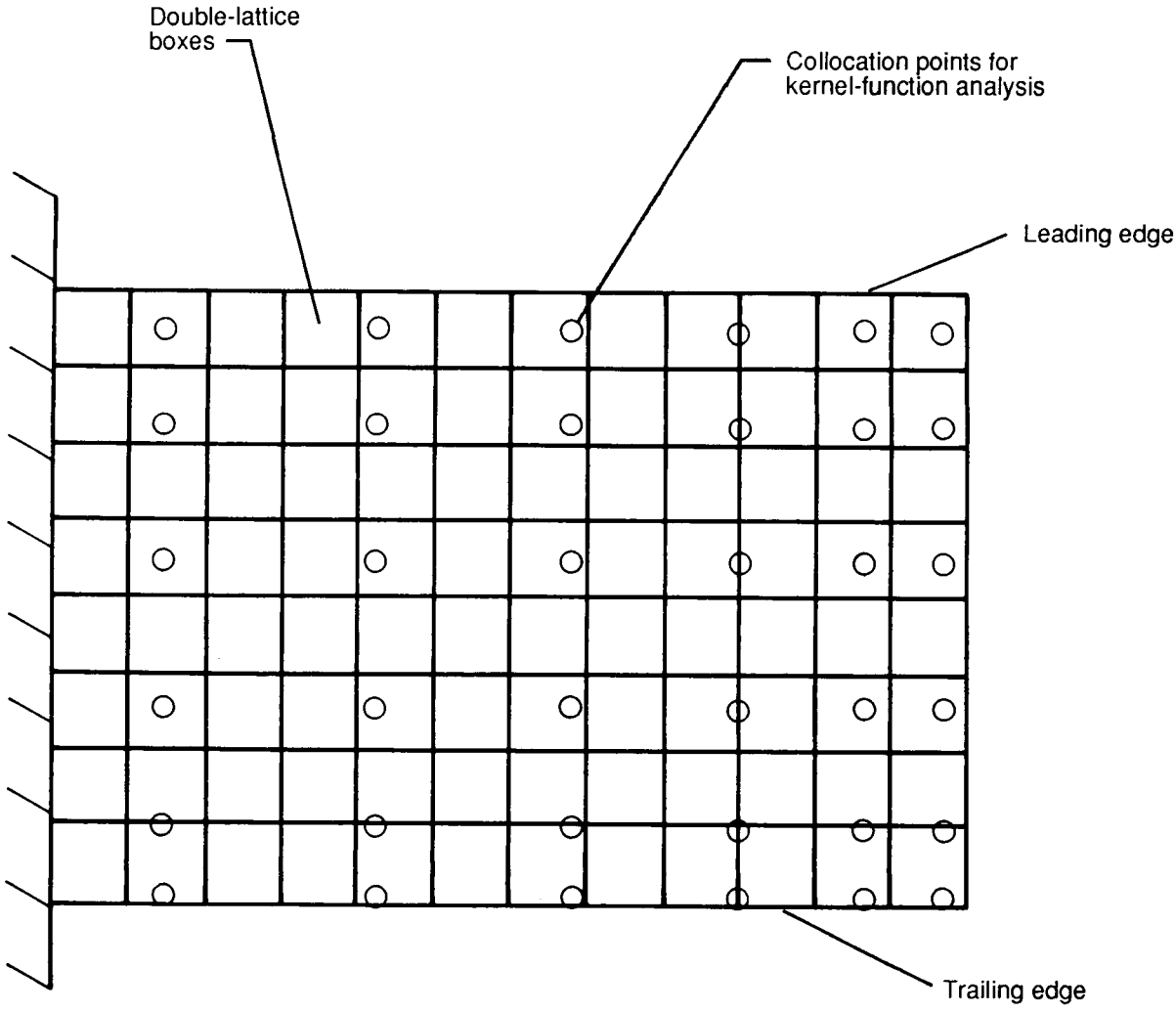

Figure 11. Aerodynamic model.

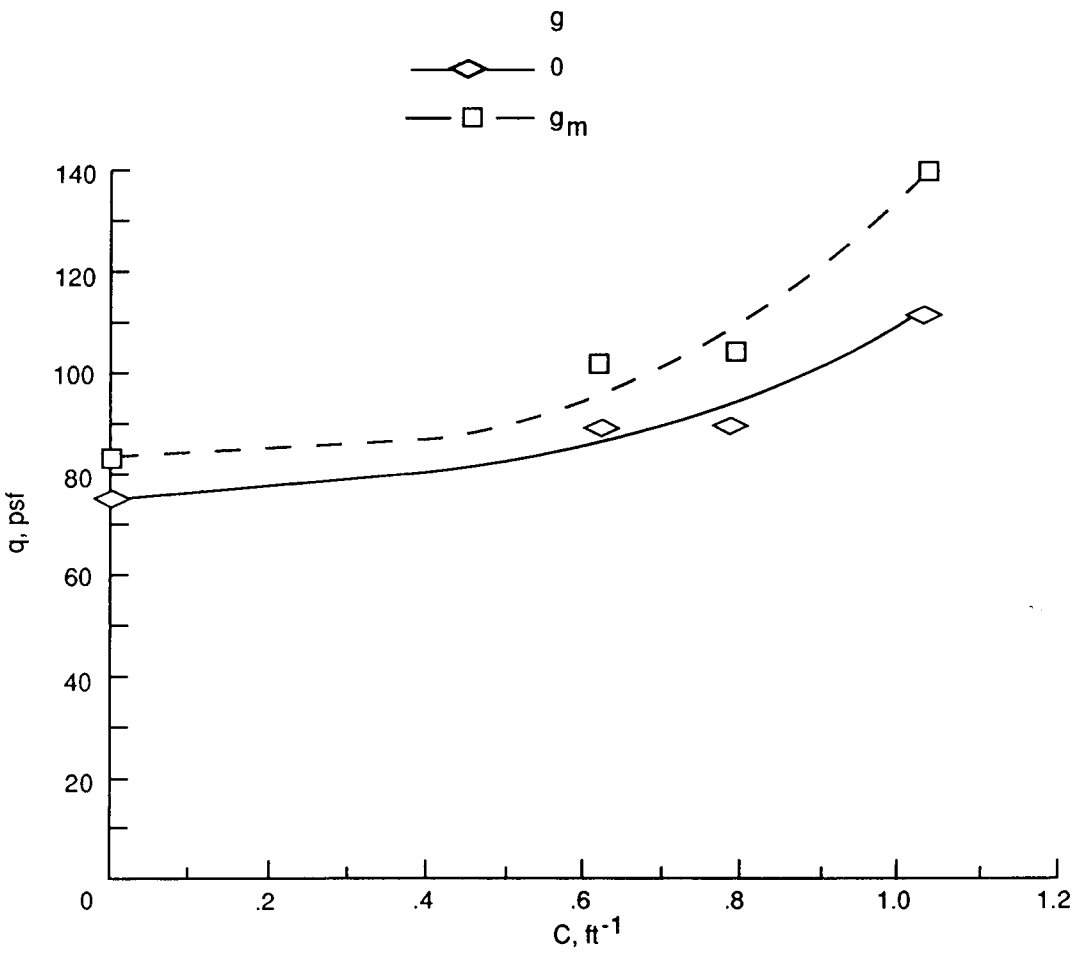

Figure 12. Effect of structural damping on analytical results for NACA 65A010 models.

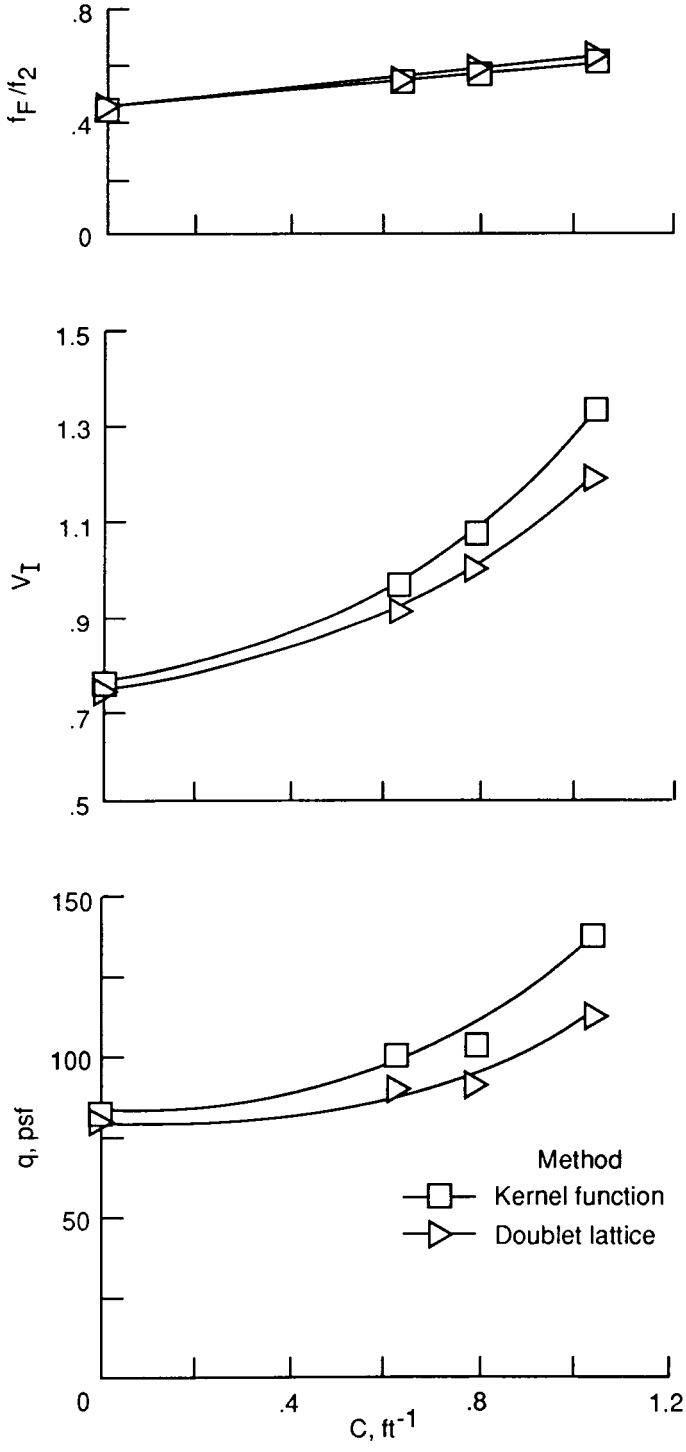

Figure 13. Analytical results for NACA 65A010 cross-section models.

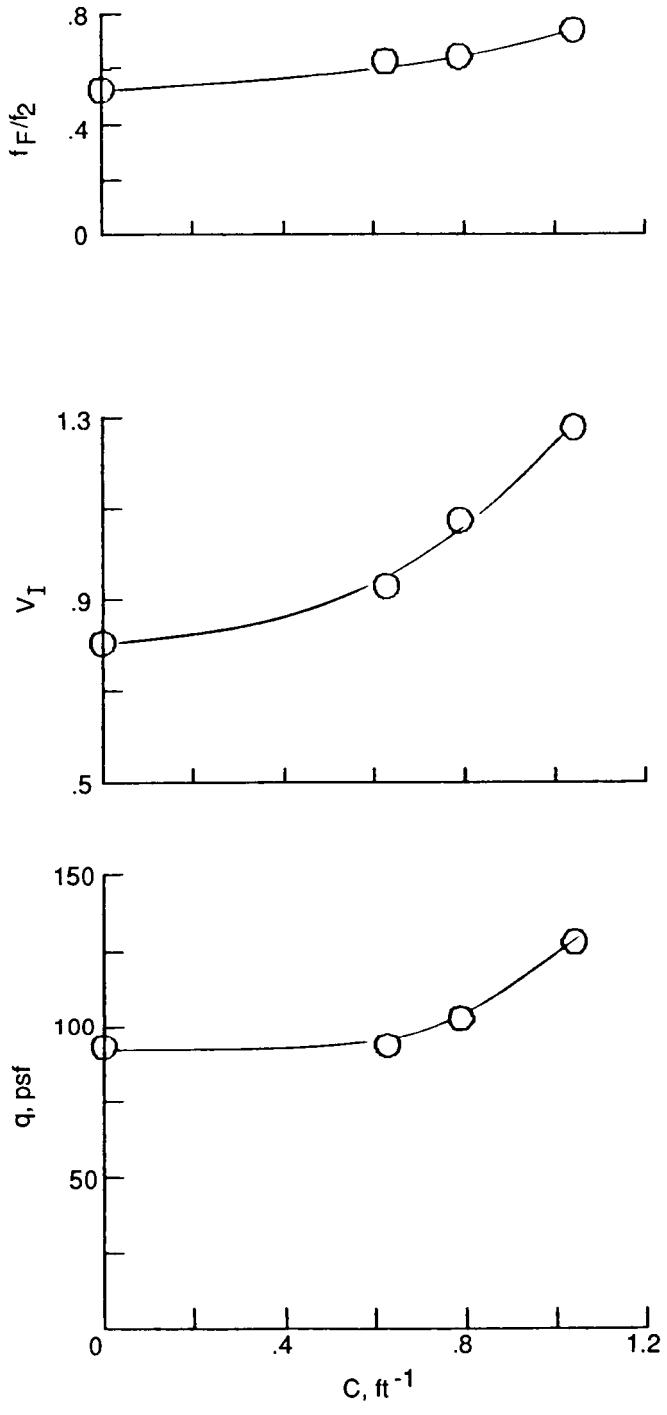

Figure 14. Experimental results for NACA 65A010 cross-section models at $M = 0.7$.

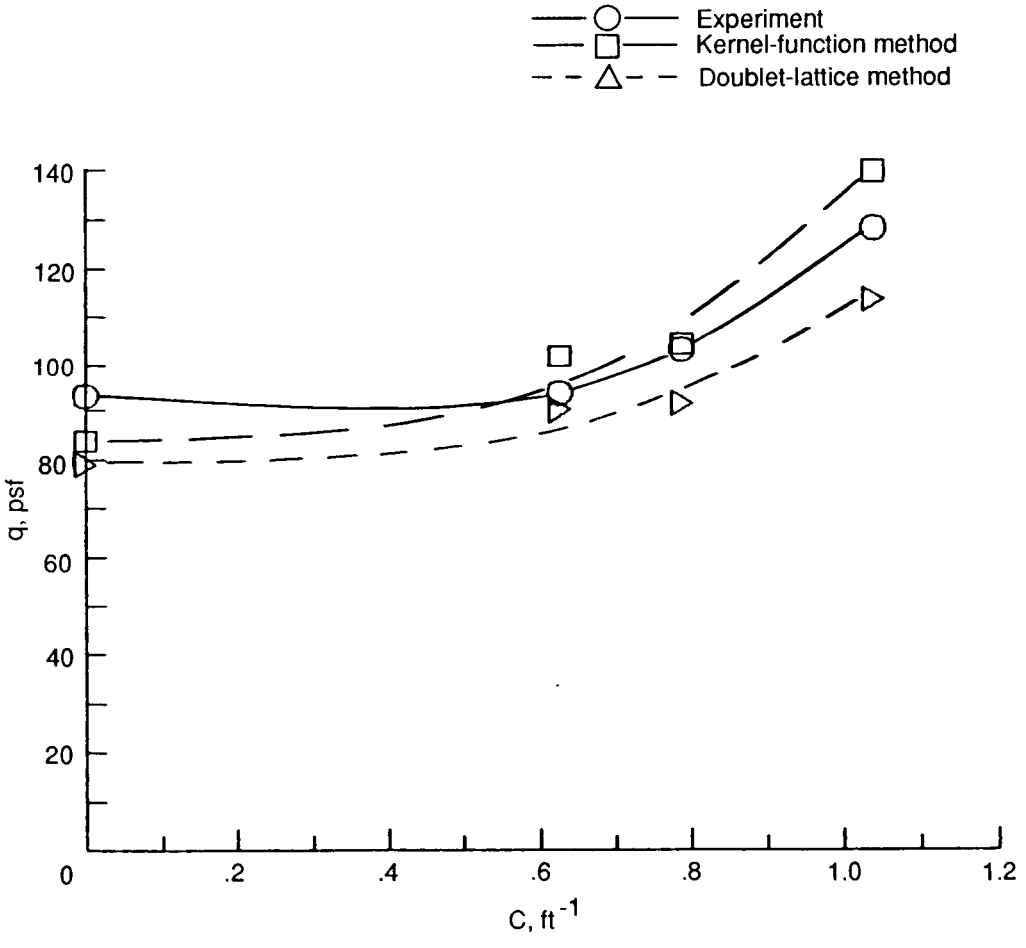

Figure 15. Experimental and analytical flutter dynamic pressure results for NACA 65A010 cross-section models at $M = 0.7$.

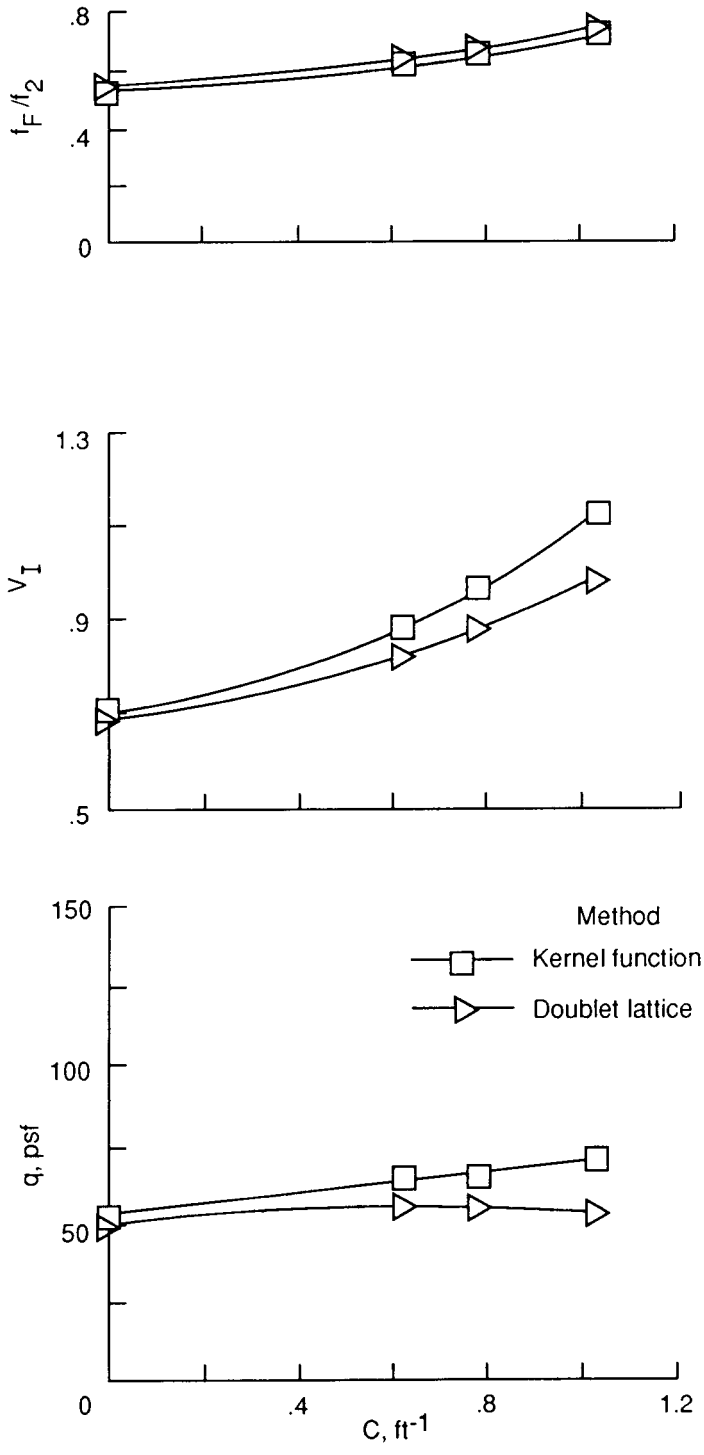

Figure 16. Analytical results for flat-plate cross-section models.

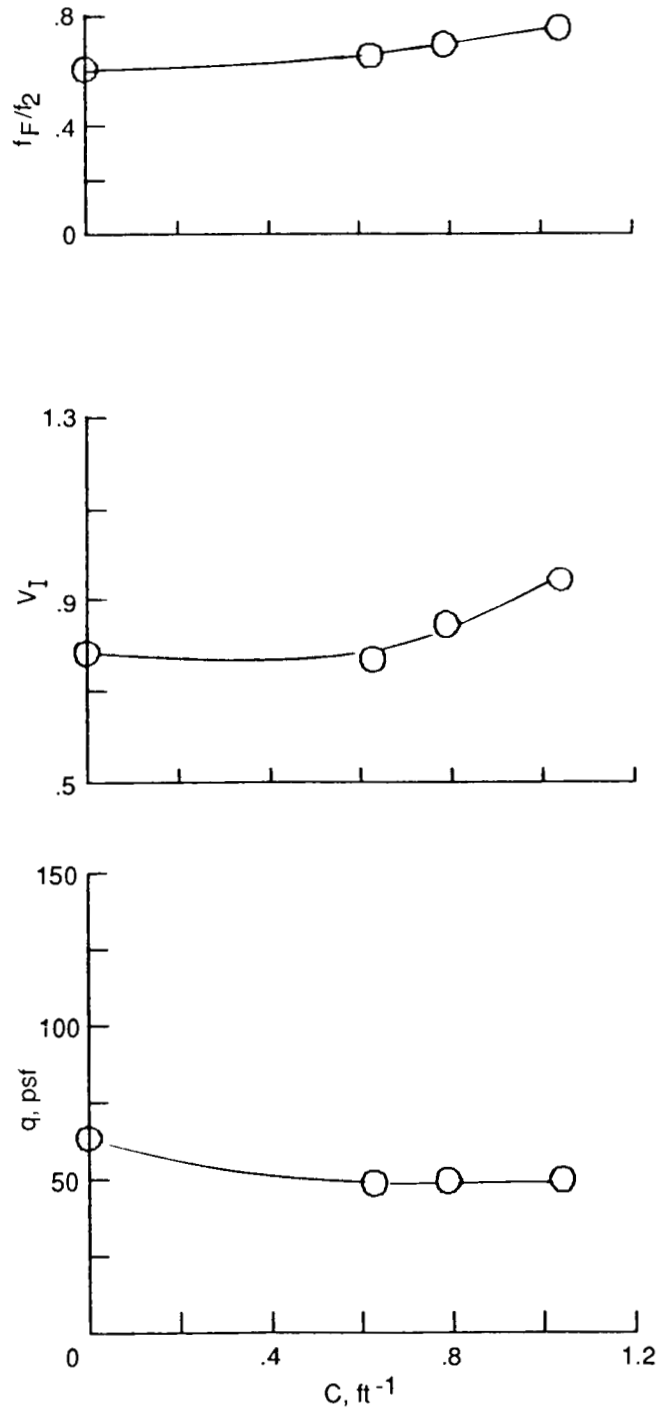

Figure 17. Experimental results for flat-plate cross-section models at $M = 0.7$.

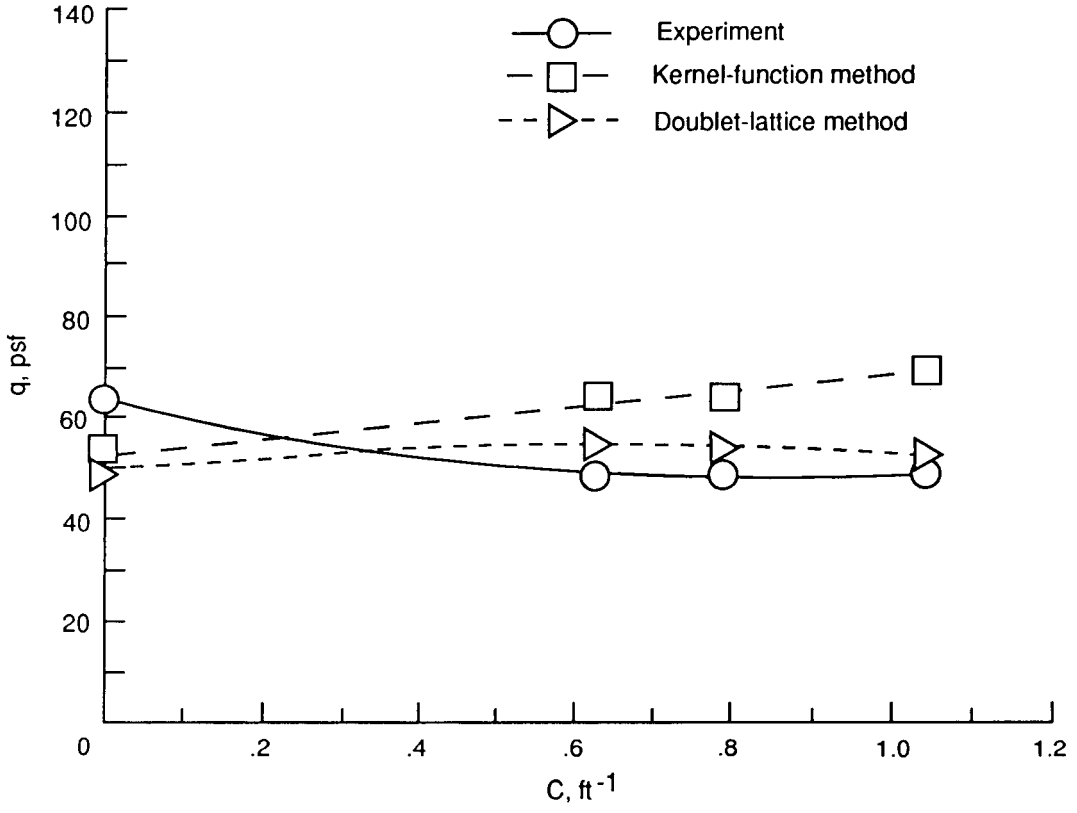

Figure 18. Experimental and analytical flutter dynamic pressure results for flat-plate cross-section models at $M = 0.7$.

NASA
National Aeronautics and Space Administration

Report Documentation Page

1. Report No.	2. Government Accession No.	3. Recipient's Catalog No.
NASA TM-4094		

4. Title and Subtitle	5. Report Date
Experimental and Analytical Investigation of the Effect of Spanwise Curvature on Wing Flutter at Mach Number of 0.7	February 1989
	6. Performing Organization Code
7. Author(s)	8. Performing Organization Report No.
Jose A. Rivera, Jr.	L-16291
	10. Work Unit No.
9. Performing Organization Name and Address	505-63-21-02
NASA Langley Research Center Hampton, VA 23665-5225	11. Contract or Grant No.
	13. Type of Report and Period Covered
12. Sponsoring Agency Name and Address	Technical Memorandum
National Aeronautics and Space Administration Washington, DC 20546-0001	14. Sponsoring Agency Code

15. Supplementary Notes

16. Abstract

An experimental and analytical study was conducted at a Mach number of 0.7 to investigate the effect of spanwise curvature on flutter. Two series of rectangular planform wings of aspect ratio 1.5 and curvature ranging from 0 (uncurved) to 1.04 ft^{-1} were flutter tested in the Langley Transonic Dynamics Tunnel. One series consisted of models with an NACA 65A010 airfoil section and the other of flat-plate cross-section models. Flutter analyses were conducted for correlation with the experimental results by using structural finite element methods to perform vibration analyses and two aerodynamic theories to obtain unsteady aerodynamic load calculations. The experimental results showed that for one series of models the flutter dynamic pressure increased significantly with curvature, whereas for the other series of models, the flutter dynamic pressure decreased with curvature. The flutter analyses, which generally predicted the experimental results, indicated that the difference in behavior of the two series of models was primarily due to differences in their structural properties.

17. Key Words (Suggested by Authors(s))
Aeroelasticity
Flutter
Spanwise curvature
Wrap-around fins

18. Distribution Statement
Unclassified—Unlimited

Subject Category 05

19. Security Classif.(of this report)	20. Security Classif.(of this page)	21. No. of Pages	22. Price
Unclassified	Unclassified	26	A03